*Journal of Sound and Vibration* (1999) **224** (3), 411–430
*Article No.* jsvi.1998.2189, available online at http://www.idealibrary.com on IDEAL®

# IMPACT TESTING OF STEREOLITHOGRAPHIC MODELS TO PREDICT NATURAL FREQUENCIES

J. P. MAHN

*Emerson Motor Company, Motor Technology Center*, 8050 *West Florissant, St. Louis, MO* 63136, *U.S.A.*

AND

P. V. BAYLY

*Mechanical Engineering, Washington University, St. Louis, MO* 63130, *U.S.A.*

(*Received* 22 *December* 1997, *and in final form* 28 *December* 1998)

Stereolithography (SLA) is a rapid-prototyping method which is used primarily to display the three-dimensional geometry of designed parts. In this paper, impact testing of SLA models is examined as a tool for the prediction of the natural frequencies of prototype aluminum parts. If the SLA model is ideal, its frequencies and those of the corresponding aluminum prototype will be related by simple ratios of material parameters and dimensions. However, the effects of properties of the SLA model which are non-ideal or qualitatively different from aluminum have not been examined. Impact tests of SLA beams, plates, and complex shapes (models of motor end shields) were performed to quantify the effects of differences such as increased mass loading (due to the lightness of SLA parts), possible anisotropy due to the "laminated" nature of the model, and mismatches between the damping, non-linearity, and the Poisson ratio of the SLA material and the corresponding properties of aluminum. The natural frequencies predicted from SLA models were compared to those measured from corresponding aluminum parts. Comparisons generally showed good agreement and suggest that carefully performed impact testing of SLA models is a useful method to predict the natural frequencies of prototype parts. These predictions may be used directly in the design process, or to validate and refine finite-element models. 

## 1. INTRODUCTION

In response to the demand for quieter machines, manufacturers are increasing the amount of noise analysis performed on their products. A part of the noise analysis may include prediction of the natural frequencies of the components of the product. Current methods of prediction include finite-element analysis (FEA). However, FEA performed on a complicated geometry can be time-consuming to model, to mesh, and to analyze. Furthermore, accurate results require the skills of an experienced analyst and even then, the accuracy of the results may be questionable.

0022-460X/99/280411 + 20 $30.00/0 

An experimental, preproduction tooling method to validate FEA results for complex geometries is needed.

In this paper, we investigate the use of stereolithographic (SLA) models as tools for validation. Since SLA models are representations of the actual parts, they can potentially be used to predict the vibrational behavior of the actual parts. Previous studies in this area include the work of Dornfeld [1], who found the relationship between the natural frequencies of aluminum turbine blades and corresponding SLA models to be dependent on the modulus of elasticity, the density and the reference length of each. The relationship was verified by testing models of turbine blades on a shaker table.

The present paper further explores practical issues in the prediction of modal properties of aluminum prototypes using impact testing of SLA models. Since impact tests can be performed quickly, the use of SLA models to predict the natural frequencies of parts would be a convenient means of rapid validation and iterative refinement of FEA models. The adverse effects of mass loading, anisotropy, damping and non-linearities in the material are all considered. Tests were conducted on beams, plates and complex parts. The plates and complex parts differ from the beams in that they may also be affected by differences in the Poisson ratio. The results indicate that impact testing SLA models is a valuable method for preproduction testing.

## 2. THEORY

Vibration problems are often studied by constructing and testing scale models. The model is a representation of a physical system which can be used to predict the behavior of the system. The physical system is referred to as the prototype. Although the behavior of the prototype may be determined by a mathematical or finite-element model, the models used for this paper are physical models.

The theory of models states that dimensionless groups of variables found by non-dimensionalizing the equations of motion of a system are equated between the model and the prototype [2, 3]. A transformation of all of the quantities in the equation of motion into a set of dimensionless parameters leads to a system equation which is independent of size and therefore applies directly to both the prototype and the model.

For example, consider the equation of motion from the Euler–Bernoulli theory for transverse vibrations of a uniform beam [4]:

$$EI\frac{\partial^4 y(x,t)}{\partial x^4}+\rho A\frac{\partial^2 y(x,t)}{\partial t^2}=0, \tag{1}$$

where $E$ is the modulus of elasticity, $I$ is the area moment of inertia of the cross-section, $y$ is the displacement, $\rho$ is the density, and $A$ is the cross-sectional area as shown in Figure 1. The variables in equation (1) can be rewritten as the dimensionless relations

$$\varepsilon=\frac{x}{l},\quad \eta=\frac{y}{l},\quad \tau=\frac{ct}{l},\quad \kappa=\frac{k}{l},\quad \alpha=\frac{A}{l^2}, \tag{2}$$

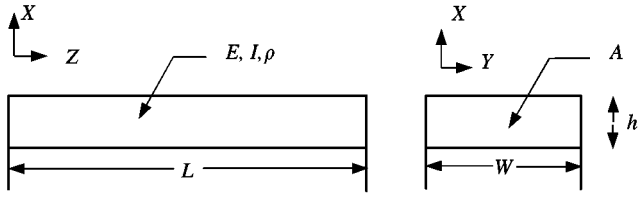


Figure 1. Side and front views of a beam used for testing.

where $c = \sqrt{E/\rho}$ is the velocity of propagation of small disturbances in the material, $k$ is the radius of gyration about the neutral axis ($k = h^2/12 = I/A$ for a uniform beam), and $l$ is the reference length [i.e. the length of the beam ($L$)]. By substituting the dimensionless relations of equation (2) into equation (1), the equation of motion becomes

$$\kappa^2 \frac{\partial^4 \eta}{\partial \varepsilon^4} + \frac{\partial^2 \eta}{\partial \tau^2} = 0. \tag{3}$$

The theory of models states that the measured value of the dimensionless parameters in equation (3) will be equal for both the model and the prototype. Therefore,

$$(ct/l)_m = (ct/l)_p. \tag{4}$$

Substituting for the velocity of propagation, $c$, and writing the frequency of vibration, $f$ as the inverse of time yields a relation between the frequencies of the model and the prototype:

$$f_p = f_m \left(\frac{l_m}{l_p}\right)\left(\frac{\sqrt{E_p/\rho_p}}{\sqrt{E_m/\rho_m}}\right) \tag{5}$$

which is dependent on the square root of the material ratio $E/\rho$ and the reference length ($l$) of both systems.

Equation (5) gives the relationship between the frequencies of the model and the prototype based on the equations of motion for transverse vibrations in a beam. This equation is valid if both model and prototype are linear, undamped and isotropic.

The equation of motion for transverse vibrations in a thin plate shows an additional dependence on the Poisson ratio. Consider the equation of motion for transverse vibration in a plate:

$$w_{xxxx} + w_{yyyy} + 2w_{xxyy} + \frac{12\mu(1 - v^2)}{Eh^3} w_{tt} = 0, \tag{6}$$

where $w$ is the deflection, $\mu$ is the mass per unit area (density/thickness), $v$ is the Poisson ratio and $h$ is the thickness. For the case of a square plate, the variables in equation (6) can be rewritten as the dimensionless quantities

$$\varepsilon = \frac{x}{l}, \quad \eta = \frac{y}{l}, \quad \kappa = \frac{w}{l}, \quad \tau = \frac{ct}{l}, \quad \beta = \frac{h}{l}, \tag{7}$$

where $c = \sqrt{E/\rho(1-\nu^2)}$ is the velocity of propagation of compressed waves in the plate [5] and $l$ is the reference length which in the case of the square plates is the width. Substituting the relations in equations (7) into equation (6) yields the non-dimensionalized equation of motion,

$$\kappa_{\varepsilon\varepsilon\varepsilon\varepsilon} + \kappa_{\eta\eta\eta\eta} + 2\kappa_{\varepsilon\varepsilon\eta\eta} + (3/\beta^2)(1-\nu^2)\kappa_{\tau\tau}. \tag{8}$$

Therefore, according to the theory of models

$$(ct/l)_m = (ct/l)_p. \tag{9}$$

Substituting into equation (9) the expression for $c$ yields the relationship between the frequencies of the model and prototype:

$$f_p = f_m \left(\frac{l_m}{l_p}\right)\left(\frac{\sqrt{E_p/\rho_p(1-\nu_p^2)}}{\sqrt{E_m/\rho_m(1-\nu_m^2)}}\right) \tag{10}$$

which shows a dependence on the modulus of elasticity, the Poisson's ratio, the density, and the reference length of each.

## 3. METHODS

### 3.1. MODAL ANALYSIS PROCEDURE

In order to use the relationship between the model and the prototype to predict the natural frequencies, the material properties of each needs to be known. The modulus of elasticity and the density of the prototype material, 6061 aluminum were $E = 70\,\text{GPa}$ and $\rho = 2710\,\text{kg/m}^3$ [6]. However, the properties of the SLA material were not published by the manufacturer and had to be determined experimentally.

The ratio of the modulus of elasticity to density was found by the vibrating beam method [7]. The method is based on the elastic theory of vibrating beams which relates the material properties to the frequencies of transverse vibrations in beams,

$$\frac{E}{\rho} = \frac{A}{I}\left(\frac{f_i}{\beta_i^2}\right)^2, \tag{11}$$

where $f_i$ is the $i$th natural frequency and $\beta_i$ is a constant dependent on the boundary conditions.

Therefore, the material ratio can be determined by inducing a test beam to vibrate in its transverse models and measuring the natural frequencies. To ensure that the correct value of $\beta_i$ was used, modal analysis was done on the beams to determine the corresponding mode shape for each natural frequency. The experimental mode shapes were then compared to the theoretical mode shapes.

The experimental set-up used to find the material properties is shown in Figure 2. The free–free boundary condition was approximated by suspending the beam by an elastomeric band as shown in the figure. Although the use of the elastomer allowed for the existence of "rigid-body" modes, the frequencies of these modes were much lower than the frequencies of the flexible modes and were therefore easily separated [8].

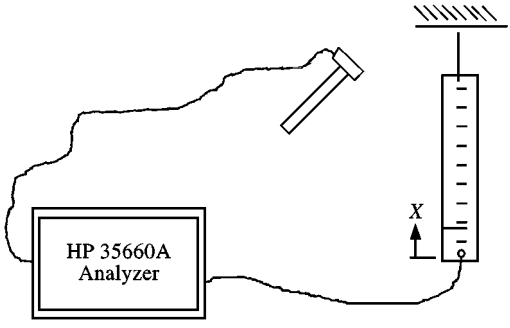


Figure 2. Experimental set-up used for determining the natural frequencies of the test beams. The beams were suspended by an elastomer to approximate the free–free boundary condition. A PCB 0·5 g accelerometer was attached to the beam with beeswax. The accelerometer and impact hammer were connected to a HP35660A analyzer.

A 0.5 g accelerometer, PCB model 352B22, was attached to the beam with beeswax. The beam was struck with an instrumented impact hammer, PCB model 086A03 at intervals of 12.7 mm allowing the evaluation of the transfer function. Three impacts were done at each point and averaged by the HP 35660A analyzer. The frequency range was 0–1600 Hz.

### 3.2. TEST SUBJECTS

The beams chosen for testing were 203.20 mm long, 25.40 mm wide and 6.35 mm high and were made from both an acrylic material, Cibatool SL5149 ($SL_{ACRYLIC}$) and an epoxy material, Cibatool SL5170 ($SL_{EPOXY}$). The SLA beams were created when the liquid resin was cured layer upon layer by the SLA machine. The resulting model has layers perpendicular to the build direction. Since the models are built in three-dimensional space, the models can be built in a variety of orientations and therefore have a variety of different layering directions. The orientation of the layers was thought to possibly be important for two reasons. Firstly, some polymers may be anisotropic [9]. Secondly, even if the average material properties are isotropic, the process of curing the models layer upon layer (the "build" process) may introduce anisotropy.

To determine if this also held true for the SLA materials, beams of different build orientations were tested. The three possible build orientations shown in Figure 3 depend on how the solid model is built with respect to the platform of the SLA machine. For the $Z$ orientation, the beams were built straight up from the platform, for the $Y$ orientation the beam was built lying directly on the platform, and for the $X$ orientation the beam was built on its side.

Ten beams for each build orientation were built of both materials. Different orientations resulted in a different degree of deviation from the nominal dimensions as shown in Table 1. The deviations were caused by tolerances in the build and by residual support structure. The $SL_{ACRYLIC}$ material resulted in the largest deviations from nominal dimensions and proved difficult to work with. The deviations were

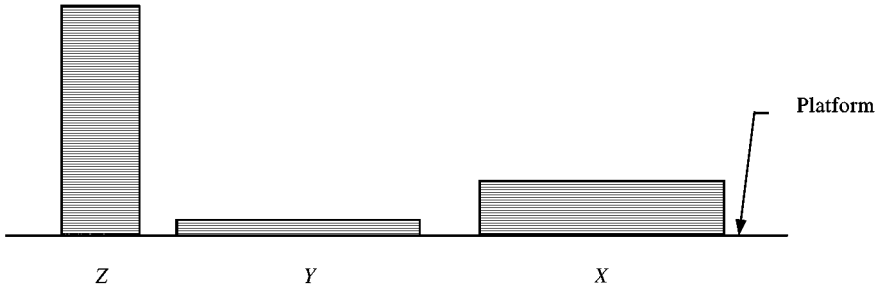


Figure 3. The beams were built in three different orientations from the platform of the SLA machine. Each orientation produced a different layering in the structure as the SLA material was cured layer upon layer.

TABLE 1

*The nominal dimensions to which the models were designed and the means and standard deviations of the actual dimensions for each beam family. The largest errors occurred in the build of the $SLA_{ACRYLIC}$ beams*

| Material | Build orientation | Length (mm) | | Height (mm) | | Width (mm) | |
|---|---|---|---|---|---|---|---|
| | | Mean | $\sigma$ | Mean | $\sigma$ | Mean | $\sigma$ |
| Nominal dims. | | 203·20 | | 6·35 | | 25·40 | |
| $SLA_{ACRYLIC}$ | *X* | 204·52 | — | 6·27 | — | 25·65 | — |
| $SLA_{ACRYLIC}$ | *Y* | 202·56 | 1·22 | 6·85 | 0·27 | 25·27 | 0·07 |
| $SLA_{ACRYLIC}$ | *Z* | 204·05 | 0·06 | 6·32 | 0·01 | 25·42 | 0·01 |
| $SLA_{EPOXY}$ | *X* | 203·25 | 0·50 | 6·36 | 0·03 | 25·53 | 0·03 |
| $SLA_{EPOXY}$ | *Y* | 203·12 | 0·03 | 6·48 | 0·02 | 25·40 | 0·02 |
| $SLA_{EPOXY}$ | *Z* | 203·35 | 0·02 | 6·35 | 0·01 | 25·29 | 0·02 |

particularly noticeable in beams built in the *X* direction. The beams became bowed when they were post-cured and only one beam was acceptable for testing. Accordingly, only the $SL_{EPOXY}$ material was used in plate and part modelling.

The models for testing also included square plates which, like the beams, were built in different build orientations. The SLA plates built for the testing were made from $SL_{EPOXY}$ in the *Y* and *X*/*Z* orientations as shown in Figure 4. A plate made of 6061 aluminum was also made for the study. Each plate was 152.4 mm long, 152.4 mm wide, and 6.35 mm thick.

Since most prototypes will not have geometries as simple as a beam or a plate, the use of the modelling equation was tested on the complex geometry of a motor end shield shown in Figure 5. The end shield model was built with the legs pointed upwards away from the base plate of the SLA machine as indicated by the arrow in the figure. Therefore, the layers of the build were parallel to the face of the end shield. The end shield was selected because both an $SL_{EPOXY}$ model and an identical aluminum prototype were available for testing. Furthermore, the end shield would be a practical application of the SLA modelling technique.

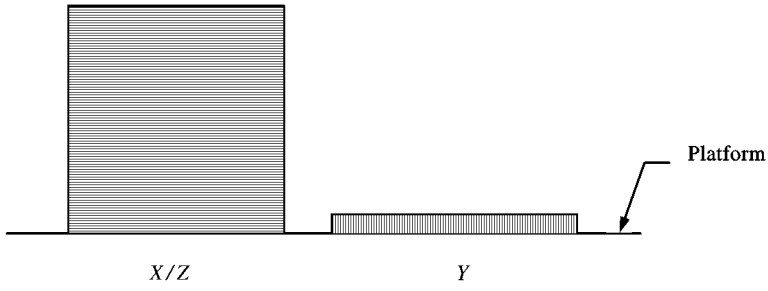


Figure 4. Square plates were built in two different orientations from the platform of the SLA machine. Each orientation produced a different layering in the structure as the SLA material was cured layer upon layer. The builds in the $X$ and the $Z$ orientations resulted in identical structures.

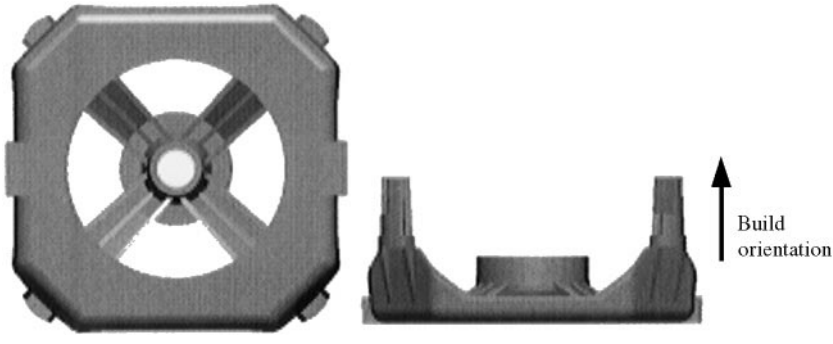


Figure 5. Top and side views of an end shield which is an example of a complex geometry. The SLA model of the end shield was built with the "legs" of the end shield pointed away from the platform of the SLA machine. The build orientation produced layering that was parallel to the face of the end shield.

### 3.3. VALIDATION OF SET-UP

Although the use of impact testing offers a simpler method of determining natural frequencies than the use of a shaker table, there were two assumptions made regarding the set-up. The first assumption was that suspending the model by an elastomeric band approximated the free–free boundary condition. This assumption was tested by comparing the results of a modal analysis on a beam of 6061 aluminum suspended by the elastomeric band to the theoretical natural frequencies and mode shapes for an identical aluminum beam with free–free boundary conditions. An aluminum beam was chosen as a test subject because the material properties are known. The resulting frequencies and flexural mode shapes are shown in Figure 6.

The results indicate a 0.52% error between the experimental and theoretical frequencies. The error may arise from the possibility that, although the average material properties of 6061 aluminum are known, there are slight differences in the material properties for each lot. The fact that the difference in the natural frequencies of modes 1 and 2 are 0.519 and 0.518%, respectively indicates that the

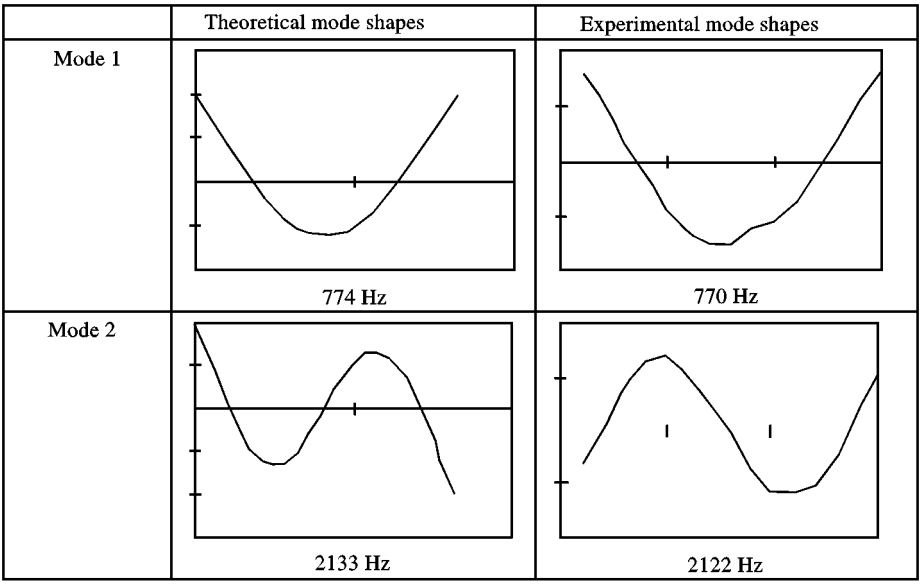


Figure 6. Flexural mode shapes and corresponding natural frequencies from theoretical and experimental results for beams. The results show a 0·52% average difference between the theoretical and the experimental frequencies for aluminum beams.

elastic modulus of the aluminum beam may be less than the average value. Because of the small error in frequency estimates, the suspension of the model by the elastomeric band was deemed an acceptable approximation of the free–free boundary conditions.

The second assumption was that the attachment of the accelerometer to the model did not significantly mass load the model. A test was conducted to determine if mass loading was present. The effect of mass loading could be determined by first recording the frequency response of the model using the accelerometer. Next, an additional accelerometer (in addition to the first) was mounted at the same point and the measurement is repeated. The two measurements were compared to determine if the addition of the second accelerometer caused any frequency shifts and amplitude changes. If the two measurements differ significantly, then mass loading is present [8]. Testing was performed using the PCB Model 352B22 0.5 g accelerometer on various models including beams, plates, and end shields.

The tests indicated that the 0.5 g accelerometer did slightly mass load the models. For example, Figure 7 shows the transfer function for an end shield. The solid line in the figure is the transfer function of the end shield with only one 0.5 g accelerometer attached. The dashed line represents the transfer function of the end shield with a second 0.5 g accelerometer attached. The addition of the second accelerometer shifted the magnitude of the natural frequencies 1 Hz for mode 1, 2 Hz for mode 2 and 2 Hz for mode 3, indicating a small amount of mass loading.

Tests performed on other geometries also showed the existence of mass loading. The ratio of average frequency shift to the unshifted frequency for the first three

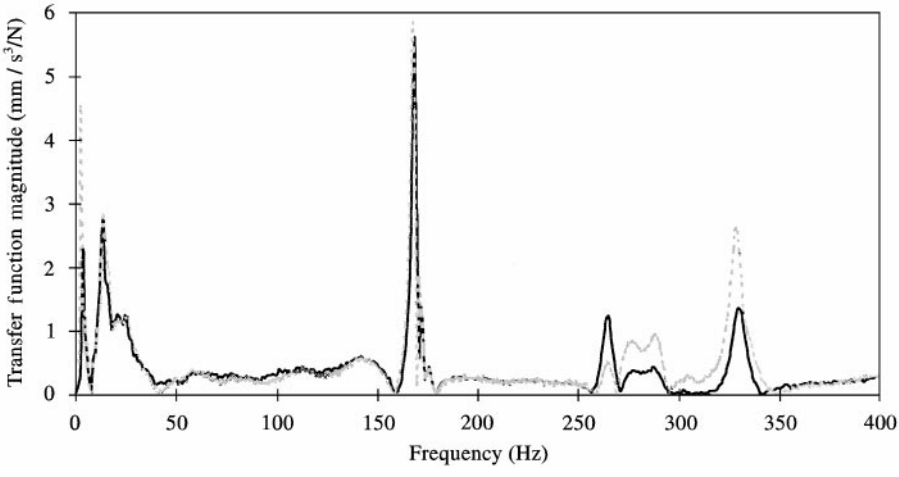


Figure 7. Comparison of unloaded and loaded transfer function for SLA end shield using 0·5 g accelerometer. The figure indicates the transfer functions measured while the additional accelerometer was or was not attached to the end shield: ——, unloaded; – – –, loaded. The frequency shift in the transfer functions is due to mass loading.

TABLE 2

*Ratio of the frequency shift to the unloaded frequency due to mass loading beams, plates, and end shields. The mass loading was due to the attachment of a* 0·5 *g PCB accelerometer to the model. The frequency shift for the first three modes are shown*

| Model | $\frac{\Delta F_{Mode\ 1}}{F_{Mode\ 1}} \times 10^3$ | $\frac{\Delta F_{Mode\ 2}}{F_{Mode\ 2}} \times 10^3$ | $\frac{\Delta F_{Mode\ 3}}{F_{Mode\ 3}} \times 10^3$ |
|---|---|---|---|
| Beam | 4·81 | 6·90 | 6·85 |
| Plate | 4·81 | 6·90 | 4·13 |
| End shield | 3·85 | 12·35 | 8·23 |

modes of beams, plates and end shields are shown in Table 2. The decrease in the ratio for the higher modes may be due to the larger amount of energy needed to excite the mass at higher frequencies. Therefore, the effect of mass loading is inversely proportional to the modal frequency. To account for mass loading, the material properties of the SLA materials were determined from the fundamental mode only which showed the least amount of shift in frequency.

## 4. RESULTS

The models were grouped by build orientation and each group was tested over a period of several weeks. The testing schedule was dictated by when build time was available in the SLA machines. In each case, the models were tested within two weeks of being built.

TABLE 3

*Means and standard deviations of material ratios from beam natural frequencies. The material ratios were the average of* 11 *samples each* (*with the exception of* $SL_{ACRYLIC}$ *built in the X direction which was for one sample only*)

| Material | Build | Mode 1 | | Mode 2 | | Mode 3 | |
|---|---|---|---|---|---|---|---|
| | | $E/\rho$ $(mm^2/s^2 \times 10^8)$ | $\sigma$ | $E/\rho$ $(mm^2/s^2 \times 10^8)$ | $\sigma$ | $E/\rho$ $(mm^2/s^2 \times 10^8)$ | $\sigma$ |
| $SL_{ACRYLIC}$ | *X* | 47·03 | — | 48·13 | — | 50·45 | — |
| $SL_{ACRYLIC}$ | *Y* | 40·57 | 2·24 | 42·23 | 2·67 | 44·16 | 3·05 |
| $SL_{ACRYLIC}$ | *Z* | 43·96 | 0·66 | 45·60 | 0·67 | 0·74 | 0·01 |
| $SL_{EPOXY}$ | *X* | 67·57 | 0·35 | 67·63 | 0·53 | 68·79 | 0·47 |
| $SL_{EPOXY}$ | *Y* | 69·30 | 1·38 | 68·53 | 1·08 | 69·70 | 0·96 |
| $SL_{EPOXY}$ | *Z* | 68·59 | 0·96 | 68·17 | 0·38 | 69·37 | 0·27 |

### 4.1. EFFECTS OF ANISOTROPY, CURING, AGING AND MATERIAL NON-LINEARITY IN BEAMS

The sampled frequency range of 0–1600 Hz allowed for the analysis of three modes of transverse vibration. The material ratio was found for each mode by substituting the frequencies and beam dimensions into the modelling relationship of equation (5). The material ratios for each mode were averaged for each family as shown in Table 3. The notations *X*, *Y*, and *Z* indicate the orientation in which the beams were built. The material ratio for the $SL_{ACRYLIC}$ beam built in the *X* direction was for one sample only due to the difficulties with the build of the $SL_{ACRYLIC}$ beams in this orientation.

The results show that the estimated material ratio of the SLA materials increased in value with increasing frequency. The increase is more predominant for the $SL_{ACRYLIC}$ material than the $SL_{EPOXY}$ material. The data indicate that the modulus of elasticity may be frequency dependent. However, since the change in the material ratio for each mode was not significant, the ratio for the fundamental model only will be used in this study.

#### 4.1.1. *Anisotropy*

The average values of the material ratios in Table 3 are slightly different for each orientation, but when the standard deviations are taken into account, the range for each family appears to encompass the range from the others. To determine if the results proved that the materials were anisotropic, the data from each beam were plotted in a probability plot. The probability plot displays the material ratio normalized to a linear probability distribution. The horizontal axis is scaled in probability and shows the percentage of the material ratio whose values is less than the data point. The vertical axis shows the range of the data variables. The means of the data sets are shown where the lines cross the 50% probability mark on the horizontal axis. The slope of each line is the standard deviation of the data set. The plot is a convenient method to distinguish and compare sets of data.

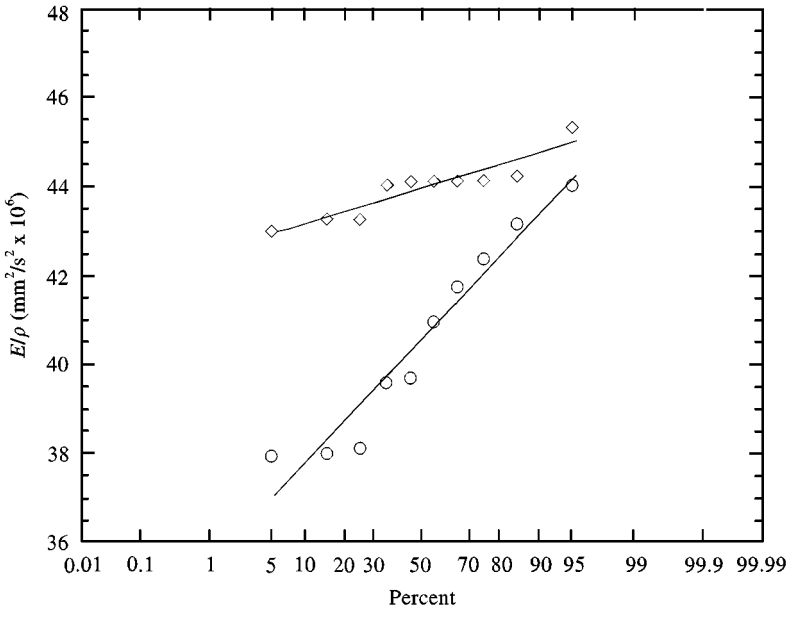


Figure 8. Probability plot of $SL_{ACRYLIC}$ material ratio for mode 1. The three different data sets are for the sets of beams built in the $X$, $Y$, and $Z$ directions: ○, $Y$; □, $X$; ◇, $Z$. There was only one beam built in the $X$ direction. The lines are a best fit for each set. The slope of the lines indicates the amount of variation in each population (see text for description of probability plot).

The probability plot for the first mode of the $SL_{ACRYLIC}$ material is shown in Figure 8. The plot shows only two distributions since there was only one data point in the $X$ orientation for the $SL_{ACRYLIC}$ material. The plot for the $SL_{ACRYLIC}$ material shows that the beams built in the $Y$ orientation had the largest standard deviation. The distributions show that the material ratios could be distinct, but the intersection of the distributions makes the results inconclusive.

The probability plot for the first mode of the $SL_{EPOXY}$ material is shown in Figure 9. Again, the largest standard deviation occurred in the $Y$ orientation. Each of the three distributions appeared to encompass points of the other distributions. The material ratios for the $X$ and $Y$ orientations could be distinct from each other, but like the $SL_{ACRYLIC}$, the results are inconclusive. The distribution for the $Z$ beams appeared to be bimodal, encompassing two distinct groups of material ratios.

The material ratio for the other vibratory modes of each material showed similar behaviors. Since the material ratios of the different orientations could not be determined to be distinct, particularly in the case of the $SL_{EPOXY}$, the materials were determined to be approximately isotropic. The material ratios for all of the orientations were averaged together to obtain one value as shown in Table 4. Each mode indicates a slightly different material ratio, again possibly due to the frequency dependence of the modulus of elasticity.

The validity of using the averaged material ratio for the fundamental mode only was tested by comparing the natural frequencies of aluminum beams predicted by using the averaged value in the modelling equation (5) to the frequencies

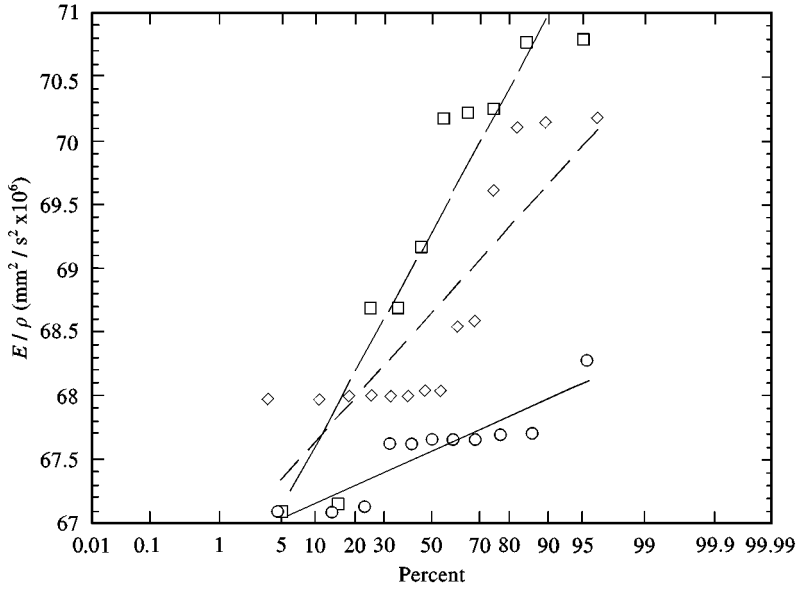


Figure 9. Probability plot of $SL_{EPOXY}$ material ratio for mode 1. The three different data sets are for the sets of beams built in the $X$, $Y$, and $Z$ directions: ○, $Y$; □, $X$; ◇, $Z$. The lines are a best fit for each set. The slope of the lines indicates the amount of variation in each population. The data shows no clear distinction between the three families (see text for description of probability plot).

TABLE 4

*Average material ratio and standard deviation for each mode of $SL_{ACRYLIC}$ and $SL_{EPOXY}$ materials*

| Material | Mode 1 | | Mode 2 | | Mode 3 | |
|---|---|---|---|---|---|---|
| | $E/\rho$ ($mm^2/s^2 \times 10^8$) | $\sigma$ | $E/\rho$ ($mm^2/s^2 \times 10^8$) | $\sigma$ | $E/\rho$ ($mm^2/s^2 \times 10^8$) | $\sigma$ |
| $SL_{ACRYLIC}$ | 42·62 | 2·54 | 44·12 | 2·67 | 46·43 | 3·00 |
| $SL_{EPOXY}$ | 68·46 | 1·19 | 68·09 | 0·79 | 69·27 | 0·72 |

determined from the theoretical equation for the natural frequency of transverse vibrations in Euler–Bernoulli beams. Therefore, the results of both equations would be for aluminum beams based on the dimensions of the SLA beam test subjects. The results from the theoretical equations were used as a baseline. The resulting errors from the modelling equation are shown in Table 5.

The comparison shows that a maximum error of 1.43% resulted between using the modelling equation with the averaged material ratio from the theoretical results. The largest errors occurred for beams built in the $Y$ orientation, potentially due to the larger amount of residual support structure this build orientation creates. The error did not increase appreciably for modes 2 and 3 despite the

TABLE 5
*Averaged error between the theoretical and predicted natural frequencies of aluminum beams. The notations X, Y, and Z indicate the build orientation*

| Beam orientation | Mode 1 % error | Mode 2 % error | Mode 3 % error |
|---|---|---|---|
| *X* | − 0·69 | 0·67 | 0·42 |
| *Y* | 1·38 | 0·57 | 1·43 |
| *Z* | − 0·34 | 0·3 | 0·6 |

TABLE 6
*Experimental natural frequencies of under- and overcured beams made of* $SL_{EPOXY}$. *The standard cure time is* 45 *min*

| Deviation from standard cure time (min) | *F*1 (Hz) Exper. | *F*2 (Hz) Exper. | *F*3 (Hz) Exper. |
|---|---|---|---|
| − 10 | 260 | 708 | 1400 |
| − 5 | 256 | 708 | 1400 |
| 0 | 256 | 708 | 1396 |
| 5 | 256 | 708 | 1396 |
| 10 | 256 | 708 | 1396 |

presence of mass loading, demonstrating that using a material ratio taken from the fundamental mode alone will probably give acceptable results for the other modes.

The use of the modelling equation was based on the assumptions that the material properties of the SLA materials were linear and did not change with age or cure time. These assumptions were tested using the natural frequencies from the SLA beams. Also investigated was the difference in the damping ratio of the SLA materials and aluminum.

4.1.2. *Variations in cure time*

The dependence of the material ratio on the post-cure time was examined by impact testing identical $SL_{EPOXY}$ beams built in the *Z* orientation and post-cured for different lengths of time. The standard post-cure time is 45 min for the beams. The range of cure times chosen for testing represent typical variations in time. The results of the tests are shown in Table 6.

Under-curing the models was expected to cause the material to have a lower modulus of elasticity, therefore lowering the natural frequencies of the beam. Likewise, over-curing was expected to cause the material to have a higher modulus of elasticity and therefore to cause the beam to have higher natural frequencies. However, the results in Table 6 show neither of these trends. The frequencies vary slightly between each beam, but the difference could be due to the variations in the

beam dimensions rather than differences in cure times. Overall, the difference of 20 min in cure time between the beams did not affect the frequencies.

#### 4.1.3. *Effect of aging*

The material properties of some materials such as plastics can change with age [10]. The implications of aging of SLA models would be that they must be tested soon after being built to ensure accurate results or the aging must be taken into account. To determine if this was the case for SLA materials, the family of $SL_{EPOXY}$ $X$ orientation beams was retested to determine if their natural frequencies had changed over time. The beams were tested on three dates with a time difference of 80 days between tests 1 and 2 and 94 days between tests 2 and 3. Although periods longer than five months could have been tested, testing so long after the SLA modes have been built would generally be beyond the useful life of the model. The main advantage of SLA models is that they can be built and tested quickly for information during the design process. Models that are older than five months may no longer accurately represent the prototype geometry or actual parts may have been tooled during this period.

The results of testing the beams showed no appreciable difference in the natural frequencies of the beams. Therefore, aging of the material does not appear to significantly affect the properties of the SLA material.

#### 4.1.4. *Non-linearities*

The modelling equation depends on the materials of both the model and the prototype to be linear. If one material was not linear, different excitation amplitudes, for examples, could result in different responses from the system.

The SLA material was considered to be potentially non-linear. Plastics exhibit material non-linearity because of their amorphous structure [9]. Furthermore, the build process could lead to inhomogeneities in the model. For example, limitation on core depth by absorption may cause inhomogeneities in the mechanical properties within the laser cured part [11]. Also, air pockets could form between layers leading to inconsistencies in the build. Two tests were performed to determine the influence of the inhomogeneities on the linearity of the SLA models.

The first test looked at the linearity of the frequency response function (FRF) of the beam. The FRF relates the input to the response by

$$|R| = |H||F|, \tag{18}$$

where $|R|$ is the response magnitude, $|H|$ is the magnitude of the FRF, and $|F|$ is the magnitude of the force. For a linear material, the magnitude of the response will be proportional to the magnitude of the force. The relationship for the SLA beam was examined by conducting 48 impact tests with forces of varying magnitudes. The set-up of the impact test was identical to that used earlier to determine the material properties shown in Figure 2. The results of the tests are shown in Figure 10. The solid line is a linear curve fit for mode 1 and the dashed line is a linear curve fit for mode 2. Despite deviations from the best fit for some impact magnitudes, the data appear to be linear.

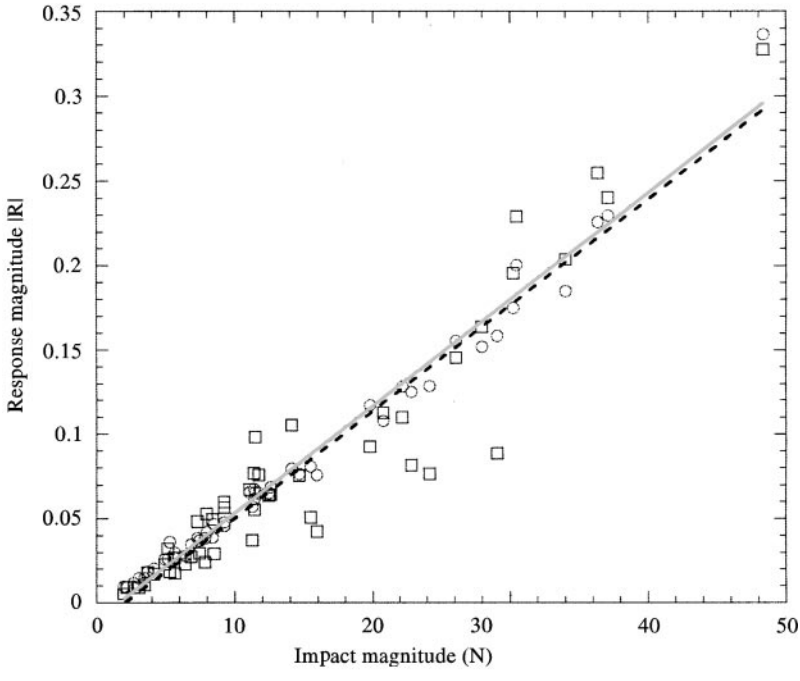


Figure 10. Magnitude of the response of the SLA versus the magnitude of the impact force for the first two modes of 48 data samples: —○—, linear fit Mode 1; - - -□- - -, linear fit Mode 2.

The second test concentrated on the assumption of linear viscous damping. Linear viscous systems have a damping which is proportional to the velocity. However, non-linear systems may show a relationship between the damping force and the velocity which is not proportional. Since the response of the system to impacts of varying magnitudes would also vary, the damping could be examined with respect to the impact magnitude. Changes in the damping for different magnitudes of excitation would show a dependence that was not proportional to velocity.

The damping ratio for the fundamental mode was determined by the use of the half-power bandwidth method [7]. The damping ratio was found for mode 1 using the experimental set-up shown in Figure 2. The damping ratio is plotted versus impact force magnitude in Figure 11. The dashed line is a linear curve fit to the data. Despite variations in the data, the damping ratio appears to remain approximately constant over the range of impact force magnitudes. The average damping ratios of the $SL_{EPOXY}$ and aluminum beams are shown in Table 7. The results also show that aluminum is more lightly damped than the $SL_{EPOXY}$ which would be expected for a comparison of a metal versus a polymer.

## 4.2. PLATES

One possible shortcoming with SLA testing is a possible mismatch of Poisson's ratios between the prototype and the model. If the Poisson's ratios were not similar,

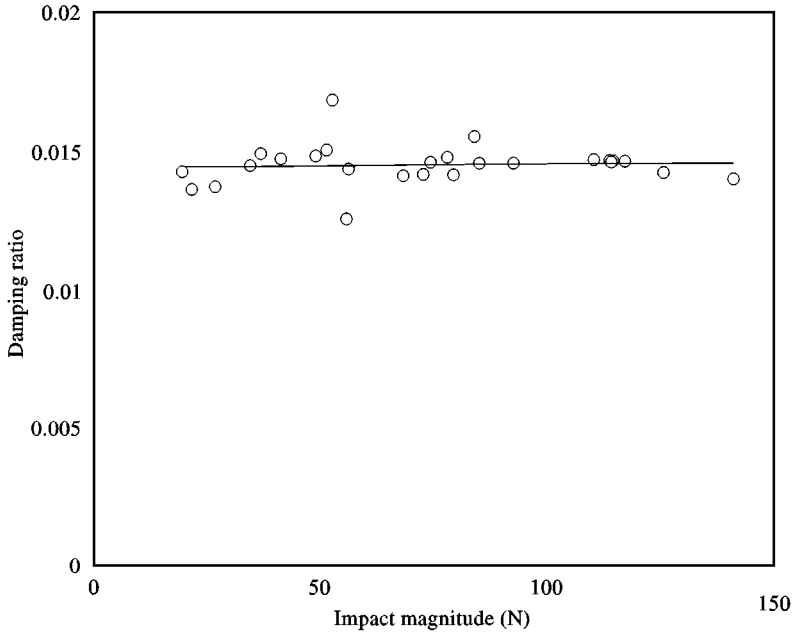


Figure 11. Damping ratio of $SLA_{EPOXY}$ versus magnitude of impact force of 26 data samples. The line is a linear curve fit to the data. The damping ratio is for mode 1 only.

TABLE 7

*Comparison of the average damping ratios of aluminum and $SL_{EPOXY}$ beams for* 28 *$SL_{EPOXY}$ samples and seven aluminum samples*

| Material | Damping ratio (%) | $\sigma$ |
|---|---|---|
| $SL_{EPOXY}$ | 1·44 | 0·25 |
| Aluminum 6061 | 0·07 | 0·01 |

errors in the predicted natural frequencies of plates or complex parts could occur. We tested two SLA plates built in different orientations and used the measured frequencies in the modelling relation (5). The predicted natural frequencies are compared to those of an aluminum plate in Table 8. The theoretical natural frequencies, derived using methods by Blevins [12] for the first three modes are 923, 1354 and 1671 Hz respectively. The low errors in the predicted frequencies show that for practical use, the Poisson ratio is approximately the same for the $SL_{EPOXY}$ and aluminum.

### 4.3. COMPLEX GEOMETRY

The end shield was built with the layers parallel to the face of the end shield as shown in Figure 5. The outer surface of the model on which the accelerometer and

TABLE 8

*Experimental and predicted natural frequencies of aluminum plate. The predictions were based on the natural frequencies of $SL_{EPOXY}$ plates built in the Y and the X/Z orientations. The data indicate that plates built in the X/Z orientation yield more accurate predictions*

| Mode | Aluminum experimental (Hz) | Aluminum predicted from *Y* orientation (Hz) | Aluminum predicted from *X/Z* orientation (Hz) | % error *Y* prediction | % error *X/Z* prediction |
|---|---|---|---|---|---|
| 1 | 855 | 898 | 860 | 4·98 | 0·60 |
| 2 | 1300 | 1359 | 1284 | 4·52 | 1·23 |
| 3 | 1642 | 1795 | 1708 | 9·32 | 4·01 |
| 4 | 2250 | 2369 | 2269 | 5·27 | 0·84 |

TABLE 9

*Comparison of experimental and predicted natural frequencies of an aluminum end shield. The SLA model was made from $SLA_{EPOXY}$. All measurements on the SLA model were made parallel to the layer structure*

| Mode | Frequency (Hz) | | % error |
|---|---|---|---|
| | Aluminum prototype | Aluminum predicted from SLA | |
| 1 | 506 | 524 | 3·47 |
| 2 | 986 | 1022 | 3·67 |
| 3 | 1410 | 1396 | − 0·98 |
| 4 | 1522 | 1558 | 2·38 |
| 5 | 1930 | 1982 | 2·70 |
| 6 | 2714 | 2792 | 2·89 |

point of impact were located was perpendicular to the layers caused by the build process. The natural frequencies of the end shield were predicted from the modelling equation and compared to the natural frequencies of an aluminum end shield. Each end shield was suspended by an elastomer. Although the frequencies most useful for noise control are those found with the part installed in the motor, the suspension by an elastomer allowed us to make a comparison between the frequencies of the two models without introducing frequencies caused by other motor components. The purpose of this testing was to make a comparison between the frequencies of the model and the prototype. The results are shown in Table 9.

The results show that accurate predictions are not limited solely to the simpler geometries of beams and plates. The modelling equation (5) used to predict the end

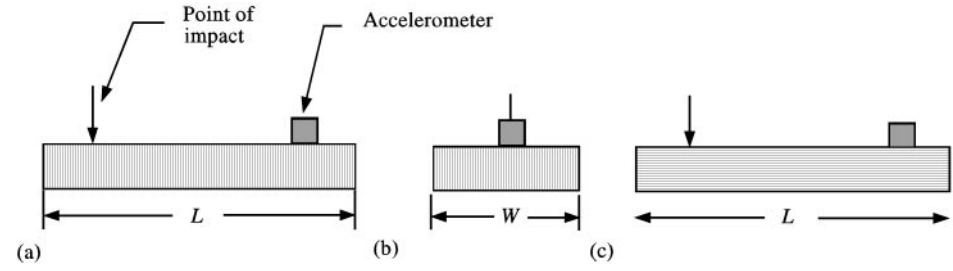


Figure 12. Views of beams built in the (a) $Z$, (b) $X$ and (c) $Y$ directions. The lines on the beam drawing indicate the orientation of the layers in the models. The arrows indicate the point where the impact load was applied. For the $X$ and $Z$ orientations, the layers are perpendicular to the surface on which the accelerometer and point of impact are located. For the $Y$ orientation, the layers are parallel to the surface.

TABLE 10

*Comparison of the natural frequencies of an end shield found from a finite-element model and an aluminum prototype*

| Mode | Experimental frequency (Hz) | FEA frequency (Hz) | % error |
|---|---|---|---|
| 1 | 506 | 520 | 2·77 |
| 2 | 986 | 1022 | 3·34 |
| 3 | 1410 | 1432 | 1·56 |
| 4 | 1522 | 1544 | 1·45 |
| 5 | 1930 | 1839 | − 4·72 |
| 6 | 2714 | 2835 | 4·46 |

shield natural frequencies was used under the implicit assumption of equal Poisson's ratios. The low errors in the resulting predictions support the claim that Poisson's ratio of the $SL_{EPOXY}$ material and the aluminum are similar. The data also indicate that the $X/Z$ orientation yields more accurate results than the $Y$ orientation. The same conclusion can be drawn from both beam and plate results. It may be important to note that in the cases of the models built in the $X$ or $Z$ directions, the layers are perpendicular to the surface on which the accelerometer and the point of impact were located. In contrast, for the $Y$ models, the layers are parallel to the surface on which the accelerometer and impact point are located (see Figure 12).

The results of a FE analysis of the same end shield using COSMOS® software are shown in Table 10. The model had 25 505 tetrahedral elements and 47 933 nodes. The FEA predicted frequencies with a maximum error of 4·72%. The errors in the FEA model could be due to geometric features such as radii being removed prior to meshing so that the model could be meshed with a reasonable number of elements. The close agreement in the results demonstrates that SLA models can be used to validate the FE models and appraise the effect of modelling assumptions.

## 5. SUMMARY AND CONCLUSIONS

The tests conducted in this study demonstrate that SLA models are a useful tool for the prediction of natural frequencies. The impact testing of models suspended by an elastomeric band is a valid procedure to find the natural frequency, despite small errors caused by mass loading. Impact testing can be easily performed and is relatively fast and inexpensive compared to modal analysis with shaker systems. Mass loading was accounted for by determining the material properties from the fundamental mode, since mass loading had a negligible effect on this mode.

A comparison of the predicted natural frequencies to the theoretical natural frequencies of beams indicated that the averaging of the material ratios did not increase the error in the predicted frequencies. Testing revealed that the SLA material is approximately isotropic and linear and that its material properties do not vary significantly with cure time or aging. Better accuracy in the predictions may be obtained by building models so that the layers due to the build process are perpendicular to the surface to which where the accelerometer will be attached.

The addition of the Poisson ratio to the modelling equation will eliminate possible errors due to a mismatch of values between the model and the prototype. However, the relatively low errors for the predicted frequencies of plates suggested that the Poisson's ratio of the $SL_{EPOXY}$ and the aluminum were similar. Future work will include direct determination of the shear modulus by finding the frequencies of the torsional modes.

For practical reasons, the $SL_{EPOXY}$ material was superior to the $SL_{ACRYLIC}$ material. Accurate natural frequency predictions using the $SL_{ACRYLIC}$ material might be difficult to achieve due to the large difference in the values of the material ratio for different modes due to the frequency-dependent behavior. The large difference would cause errors in the prediction of natural frequencies, since the material ratios used in the modelling equation are based on the fundamental mode only. Furthermore, with the $SL_{ACRYLIC}$ material it proved difficult to make accurate beam samples.

The modulus of elasticity of the $SL_{EPOXY}$ material also demonstrated a possible frequency dependence. The frequency dependence might be addressed by using a different material ratio for each mode.

SLA models can be expensive to make, with costs reaching up into the thousands of dollars for large models. However, full size models are not necessary to make use of the modelling equation. The scale between the prototypes and the models in this study was 1 : 1, but this does not always need to be the case. Models of smaller scale could be used, as long as the model was of sufficient size and mass to perform accurate impact tests. However, the cost of making SLA models is small when compared to the expense of changing incorrect tooling which was based on incorrect analytical or numerical predictions. FEA must be done by a skilled analyst using an accurate model and mesh. Widely differing results can be obtained from FEA depending on how accurately the modelling and meshing are done and how well the results are interpreted. On the other hand, impact testing of SLA models will consistently yield the same natural frequencies. Impact testing of $SL_{EPOXY}$ models appears to be a valuable method for the prediction of natural frequencies, either alone or to validate FE results.

## REFERENCES

1. W. H. Dornfeld 1995 *Sound and Vibration* **29**, 12–17. Direct dynamic testing of scaled stereolithographic models.
2. L. Sedov 1959 *Similarity and Dimensional Methods in Mechanics*. New York: Academic Press.
3. M. Hetenyi 1950 *Handbook of Experimental Stress Analysis*. New York: Wiley.
4. A. W. Leissa 1973 *Journal of Sound and Vibration* **31**, 257–293. The free vibration of rectangular plates.
5. H. Chu and G. Hernan 1956 *Journal of Applied Mechanics* **23,** 532. Influence of large amplitudes on free flexural vibrations of rectangular elastic plates.
6. F. P. Beer and E. R. Johnson 1992 *Mechanics of Materials*. New York: McGraw-Hill.
7. A. Nashif, J. G. Jones and J. P. Henderson 1985 *Vibration Damping*. New York: Wiley.
8. Hewlett-Packard 1986 *Application Note* 243-3, *Fundamentals of Modal Testing*. Englewood, CO: Hewlett-Packard.
9. Hoechst Celanese 1992 *Designing with Plastic*, *the Fundamentals*. Chatham, NJ: Hoechst Celanese.
10. W. Callister 1991 *Materials Science and Engineering*. New York: Wiley.
11. P. F. Jacobs 1992 *Rapid Prototyping & Manufacturing*, *Fundamentals of StereoLithography*. Dearborn, MI: Society of Manufacturing Engineers.
12. R. Blevins 1992 *Formulas for Natural Frequency and Mode Shape*, Malabar, FL: Kriger Publishing Co.